Crystal Structure of Yeast Acetyl-Coenzyme A Synthetase in Complex with AMP[†]

Gerwald Jogl and Liang Tong*

Department of Biological Sciences, Columbia University, New York, New York 10027

Received October 27, 2003; Revised Manuscript Received December 2, 2003

ABSTRACT: Acetyl-coenzyme A synthetase (ACS) belongs to the family of AMP-forming enzymes that also includes acyl-CoA synthetases, firefly luciferase, and nonribosomal peptide synthetases. ACS catalyzes the two-step activation of acetate to acetyl-CoA: formation of an acetyl-AMP intermediate from acetate and ATP and the transfer of the acetyl group to CoA. In mammals, the acetyl-CoA product is used for biosynthesis of long chain fatty acids as well as energy production. We have determined the crystal structure of yeast ACS in a binary complex with AMP at 2.3 Å resolution. The structure contains a large, N-terminal domain and a small, C-terminal domain. AMP is bound at the interface between the two domains. This structure represents a new conformation for the ACS enzyme, which may be competent for catalyzing the first step of the reaction. A Lys residue that is critical for this step is located in the active site. A rotation of 140° in the small domain is needed for the binding of CoA and the catalysis of the second step. In contrast to the monomeric bacterial enzyme, yeast ACS is a stable trimer.

Acetyl-coenzyme A synthetase (ACS, EC 6.2.1.1) catalyzes the formation of acetyl-CoA from acetate, CoA, and ATP (Figure 1A). This enzyme is present in most living organisms, from bacteria to humans, and has key roles in the activation and utilization of acetate, propionate, and other small organic acids. The acetyl-CoA product can be used for biosynthesis of glucose, fatty acids, and cholesterol, as well as for oxidation to produce energy in the citric acid cycle.

In bacteria, the activity of ACS, and the related propionyl-CoA synthetase (PCS), is required for growth in media with acetate, ethanol, or propionate as the sole carbon source (*1*). In yeast, two isoforms of ACS have been identified. ACS1 may be a peroxisomal enzyme and is needed for growth on C2 compounds, whereas ACS2 may be required for the production of acetyl-CoA from pyruvate via the so-called pyruvate dehydrogenase (PDH) bypass (*2*).

In mammals, there are also two isoforms of ACS. ACS1 is a cytosolic enzyme that is mostly found in the liver, and it plays an important role in providing acetyl-CoA for fatty acid and cholesterol biosynthesis (*3*). ACS1 is regulated by sterol regulatory element-binding proteins (SREBPs), which are key transcriptional factors that control the activities of many enzymes involved in fatty acid and cholesterol biosynthesis. ACS2 is present in the mitochondrial matrix and is mostly found in the heart and skeletal muscle (*4*). The acetyl-CoA produced by this isoform is primarily used for energy production in the citric acid cycle, where it is oxidized to CO_2. The activity of this enzyme is induced by starvation and other ketogenic conditions. The acetate substrate is produced from oxidation of ingested ethanol, hydrolysis of acetyl-CoA in the liver (especially under ketogenic conditions), breakdown of the neurotransmitter acetylcholine in neurons, and other sources.

The reaction catalyzed by ACS proceeds in two steps (Figure 1A). In the first step, the enzyme produces the acetyl-AMP intermediate from the acetate and ATP substrates, and pyrophosphate PP_i is released in this process. In the second step, the acetyl-AMP intermediate is reacted with CoA to produce the acetyl-CoA product and the release of AMP (Figure 1B). Consequently, ACS belongs to the superfamily of AMP-forming enzymes that also includes firefly luciferase (*5*), acyl-CoA synthetases, and nonribosomal peptide synthetases such as gramicidin synthetase (*6*).

The ACS enzyme from *Salmonella* is regulated by the acetylation of Lys609 (*7*), and this acetylation abolishes the formation of the acetyl-AMP intermediate but has no impact on the transfer of the acetyl group from acetyl-AMP to CoA. This observation also supports the two-step reaction pathway for ACS. A deacetylase of the Sir2 family is needed to keep ACS in its active form. This Lys residue is highly conserved among all AMP-forming enzymes, and is equivalent to Lys675 in yeast ACS (Figure 1B). It has been suggested that all AMP-forming enzymes may be regulated by acetylation of this Lys residue (*7*).

The crystal structure of a bacterial ACS, from *Salmonella enterica*, has recently been reported, in a ternary complex with propyl-AMP and CoA (*8*). This conformation of the enzyme is believed to be able to catalyze the second step of the reaction. We report here the crystal structure of a eukaryotic ACS, ACS1 from *Saccharomyces cerevisiae*, in a binary complex with AMP. The structure represents a new conformation for the ACS enzyme, which may be suitable for catalyzing the first step of the reaction. Major differences are observed in the positioning of the C-terminal small domain of the enzyme between the binary complex and the ternary complex. Lys675 is located in the active site in the binary complex, in agreement with its important role in the first step of the reaction. In contrast, this side chain is on the surface of the enzyme in the ternary complex, and does

[†] This research was supported by Columbia University (L.T.).

* To whom correspondence should be addressed. Phone: (212) 854-5203. Fax: (212) 854-5207. E-mail: tong@como.bio.columbia.edu.

10.1021/bi035911a CCC: $27.50
Published on Web 01/21/2004

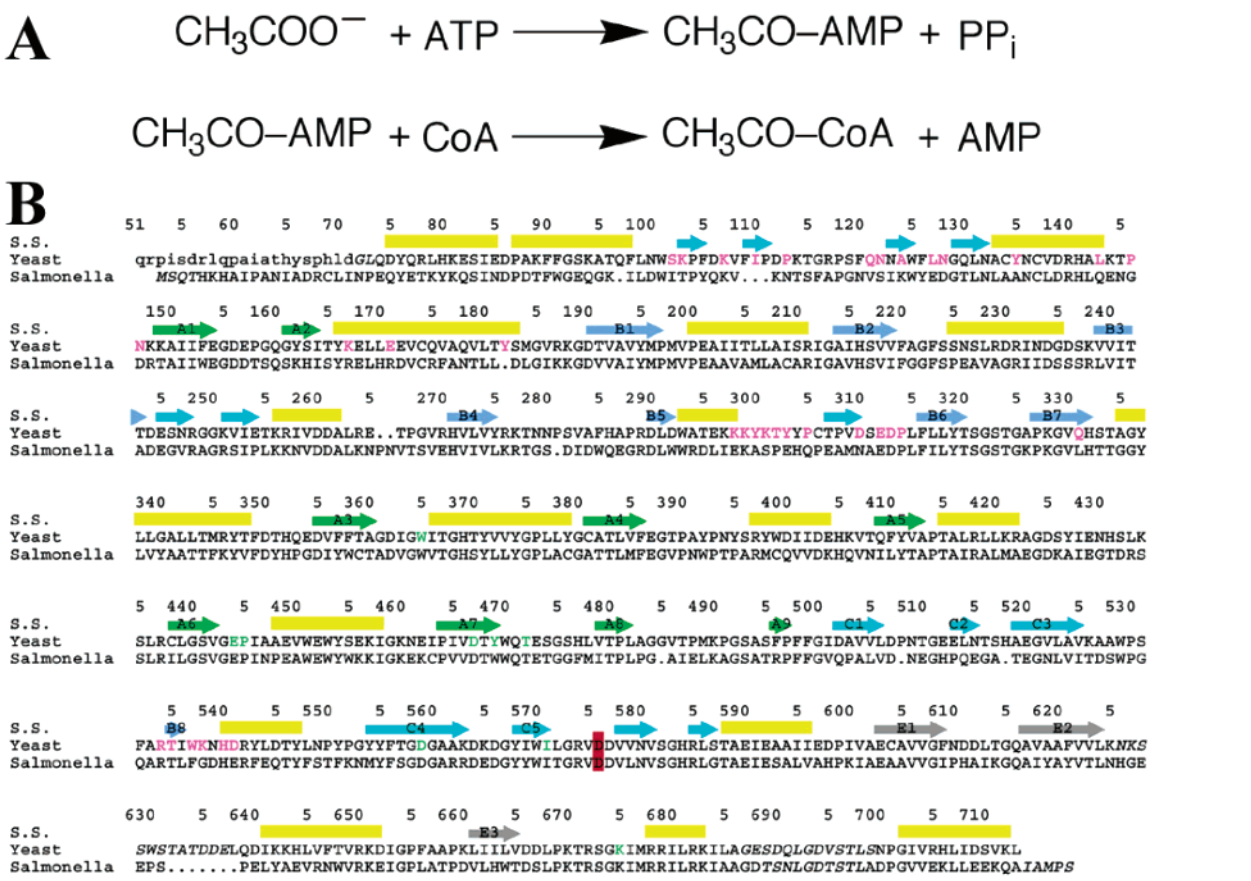

FIGURE 1: Amino acid sequences of acetyl-coenzyme A synthetases. (A) Two-step reaction catalyzed by ACS. (B) Amino acid sequence alignment of yeast and *Salmonella* ACS. The secondary structure elements in yeast ACS are indicated. Residues in the trimer interface are shown in magenta and those involved in binding AMP in green. The hinge residue (Asp576) is highlighted in red. Residues that are disordered in the crystals are shown in italics. Lowercase residues are those not included in the expression construct.

not participate in the catalysis of the second step of the reaction.

MATERIALS AND METHODS

Protein Expression, Purification, and Crystallization. Residues 72−713 of ACS from *S. cerevisiae* were subcloned into the expression vector pET28a (Novagen) and expressed in *Escherichia coli* strain BL21Star (Invitrogen). These residues are selected for the expression construct on the basis of the sequence alignment with the bacterial and other ACS homologues (Figure 1B) (*8*). The expression construct introduced a hexahistidine tag at the N-terminus, which was not removed for crystallization. The soluble ACS protein was purified by nickel agarose affinity chromatography, anion exchange, and gel filtration chromatography. The protein was concentrated to 20 mg/mL in a buffer containing 10 mM Tris (pH 8.5) and 20 mM NaCl.

Crystals of ACS were obtained at 4 °C with the sitting-drop vapor diffusion method. The best crystals appeared after 2 weeks from a reservoir solution containing 0.7 M succinic acid and 0.1 M Tris (pH 7.5). The protein concentration was 10 mg/mL, and 5 mM ATP was included in the drop. Interestingly, no crystals could be obtained when either AMP or ATP in combination with sodium acetate was used. Crystals grew to maximum dimensions of ~0.15 mm × ~0.15 mm × ~0.03 mm, and seeding experiments did not produce further improvement. For data collection, crystals were cryoprotected with the introduction of 25% (v/v) ethylene glycol and flash-frozen in liquid nitrogen.

Table 1: Summary of Crystallographic Information

	I	II
maximum resolution (Å)	2.8	2.3
no. of observations	45133	85039
R_{merge} (%)[a]	11.2 (36.9)	6.6 (24.0)
twinning fraction, $\langle I^2\rangle/\langle I\rangle$[b]	−	0.48, 1.69
resolution range for refinement	−	30−2.3
no. of reflections	−	27899
completeness (%)	96 (88)	89 (79)
R factor[b] (%)	−	19.9 (28.5)
R_{free} (%)	−	25.8 (31.9)
rms deviation in bond lengths (Å)	−	0.006
rms deviation in bond angles (deg)	−	1.3
average B values for the large domain, small domain, and AMP	−	34.4, 69.0, 35.9

[a] $R_{merge} = \sum_h\sum_i|I_{hi} - \langle I_h\rangle|/\sum_h\sum_i I_{hi}$. The numbers in parentheses are for the highest-resolution shell. [b] $R = \sum_h|F_h^o - F_h^c|/\sum_h F_h^o$.

Data Collection and Processing. The X-ray diffraction data sets were collected at National Synchrotron Light Source (NSLS) beamline X4A. The crystal belongs to space group $P3$ with the following cell parameters: $a = b = 107.1$ Å and $c = 54.8$ Å. There is one molecule of yeast ACS in the asymmetric unit. The diffraction images were recorded on an ADSC Quantum-4 CCD instrument, and processed with the HKL package (Table 1) (*9*). A weak diffraction data set to 2.8 Å resolution was collected first on a small crystal of the enzyme, which enabled the determination of the structure by the molecular replacement method. For structure refinement, a better quality data set, to 2.3 Å resolution, was collected on a larger crystal. However, crystallographic

analyses show that this crystal had almost perfect merohedral twinning, as the diffraction data set has apparent *P*321 symmetry (see below).

Structure Determination and Refinement. A homology model for yeast ACS was built from the structure of *Sa. enterica* ACS (*8*), with the program Modeller (*10*). The amino acid sequences of the two proteins are 47% identical, and the yeast ACS sequence contains several insertions and/or deletions relative to the bacterial ACS sequence (Figure 1B). This homology model was used for combined molecular replacement calculations with the program COMO (*11*). Expecting differences in the orientation of the small domain, we first determined the position of the large domain. With the information on the large domain, we located the small domain by examining a large collection of rotation angles.

The structure refinement was carried out with the program CNS (*12*), and the atomic model was rebuilt against the $2F_o - F_c$ electron density map with the program O (*13*). The diffraction data collected on the larger crystal had apparent *P*321 symmetry, and the twinning fraction was estimated to be 0.48. On the basis of the atomic model, the diffraction data set was detwinned, using standard procedures in the CNS program (*12*), and structure refinement was performed against this modified data set. Regions of ambiguous electron density were omitted from the refinement, and the atomic model was adjusted against the resulting omit electron density. The refinement statistics are summarized in Table 1.

RESULTS AND DISCUSSION

Structure Determination. The initial structure of yeast ACS was determined by the molecular replacement method (*11*), using a homology model that was built on the basis of the crystal structure of *Salmonella* ACS (*8*). The amino acid sequences of the yeast and bacterial enzymes are 47% identical, and the large domain of the yeast enzyme was readily located by the combined molecular replacement calculations (*14*). As we expect the small domains of the two enzymes to have very different orientations, the molecular replacement calculations systematically examined a significant number of orientations for the small domain, and a clear solution for the location of the small domain was obtained with this procedure.

For structure refinement, we collected a second data set, using a larger crystal. This new data set extends to higher resolution and has better quality (Table 1). However, the diffraction data have apparent *P*321 symmetry, suggesting that the crystal is almost perfectly merohedrally twinned (there can be only one molecule of ACS in the asymmetric unit in the *P*3 space group). Such a twinning problem can be easily handled using standard protocols in CNS (*12*), and the structure refinement proceeded smoothly. The crystallographic statistics are summarized in Table 1.

Overall Structure. The crystal structure of yeast ACS has been determined at 2.3 Å resolution. The current atomic model contains residues 74−713 of the enzyme, with the exception of residues 626−637 and 687−699. No electron density was observed for these residues, and they are likely disordered in these crystals. The first segment (residues 626−637) corresponds to an insertion in yeast ACS relative to the bacterial ACS (Figure 1B), whereas residues in the second segment are also disordered in the bacterial ACS structure (*8*). An AMP molecule is bound in the active site of the enzyme. The atomic model has excellent agreement with the observed diffraction data, as well as the expected bond lengths and bond angles (Table 1). Most of the residues (98%) are located in the most favored and additional allowed regions of the Ramachandran plot. Only one residue, Ser495, is located just outside the generously allowed region ($\phi = 60°$ and $\psi = -113°$). Interestingly, the residue equivalent to Ser495 in the bacterial ACS, Thr438, has a similar main chain conformation ($\phi = 74°$ and $\psi = -117°$) (*8*). The current atomic model does not contain any solvent molecules.

The structure of yeast ACS contains a large, N-terminal domain (residues 74−576) and a small, C-terminal domain (residues 577−713) (Figure 2A), like the structures of bacterial ACS and other AMP-forming enzymes (*5*, *6*, *8*). The large domain contains two mostly parallel β-sheets of nine (sheet A) and eight strands [sheet B, maintaining the nomenclature from gramicidin synthetase 1 (*6*)] (Figure 1B). These two sheets are arranged parallel to each other, and they sandwich eight helices between them. The large domain also contains an antiparallel β-sheet of five strands (sheet C) (Figure 2A), as well as several other α-helices and small β-sheets.

The electron density for residues in the small domain is much weaker than that of the large domain (Figure 3A,B), and the two peptide segments that are missing in the current atomic model are both from this domain. As in the bacterial ACS, the small domain of yeast ACS contains a three-stranded β-sheet (sheet E), together with helices on its faces (Figure 2A).

The atomic coordinates for the structure have been deposited in the Protein Data Bank (entry 1RY2).

Large Rearrangement of the Small Domain. The large domain of yeast ACS can be superimposed with that of bacterial ACS, producing an rms distance of 1.0 Å for 467 structurally equivalent Cα atoms (Figure 2B). The structural similarity between these two enzymes is consistent with their significant sequence homology (Figure 1B). The structure of the large domain of yeast ACS also is very similar to that from other AMP-forming enzymes, such as firefly luciferase (rms distance of 1.4 Å for 219 equivalent Cα atoms) (*5*) and gramicidin synthetase 1 (1.2 Å for 193 Cα atoms) (Figure 2C) (*6*). The level of amino acid sequence identity between ACS and these other two enzymes is however only 16−20%.

This structural comparison also shows that there is a significant degree of variability in the placement of the small domain in the different AMP-forming enzymes. A rotation of 137° is needed to superimpose the small domains of yeast and bacterial ACS (Figure 2B). The position of the small domain observed here for yeast ACS is closest to that in the adenylation domain of gramicidin synthetase 1, with a difference in orientation of 21° (Figure 2C). An intermediate difference is observed with the small domain of firefly luciferase, and a rotation of 80° is needed to superimpose it with the yeast ACS. It is unlikely that the conformation of the small domain observed here for yeast ACS is stabilized solely by crystal packing. In fact, the difference in the placement of the small domain is probably linked to the catalytic cycle of the enzyme (see below), as suggested previously (*8*).

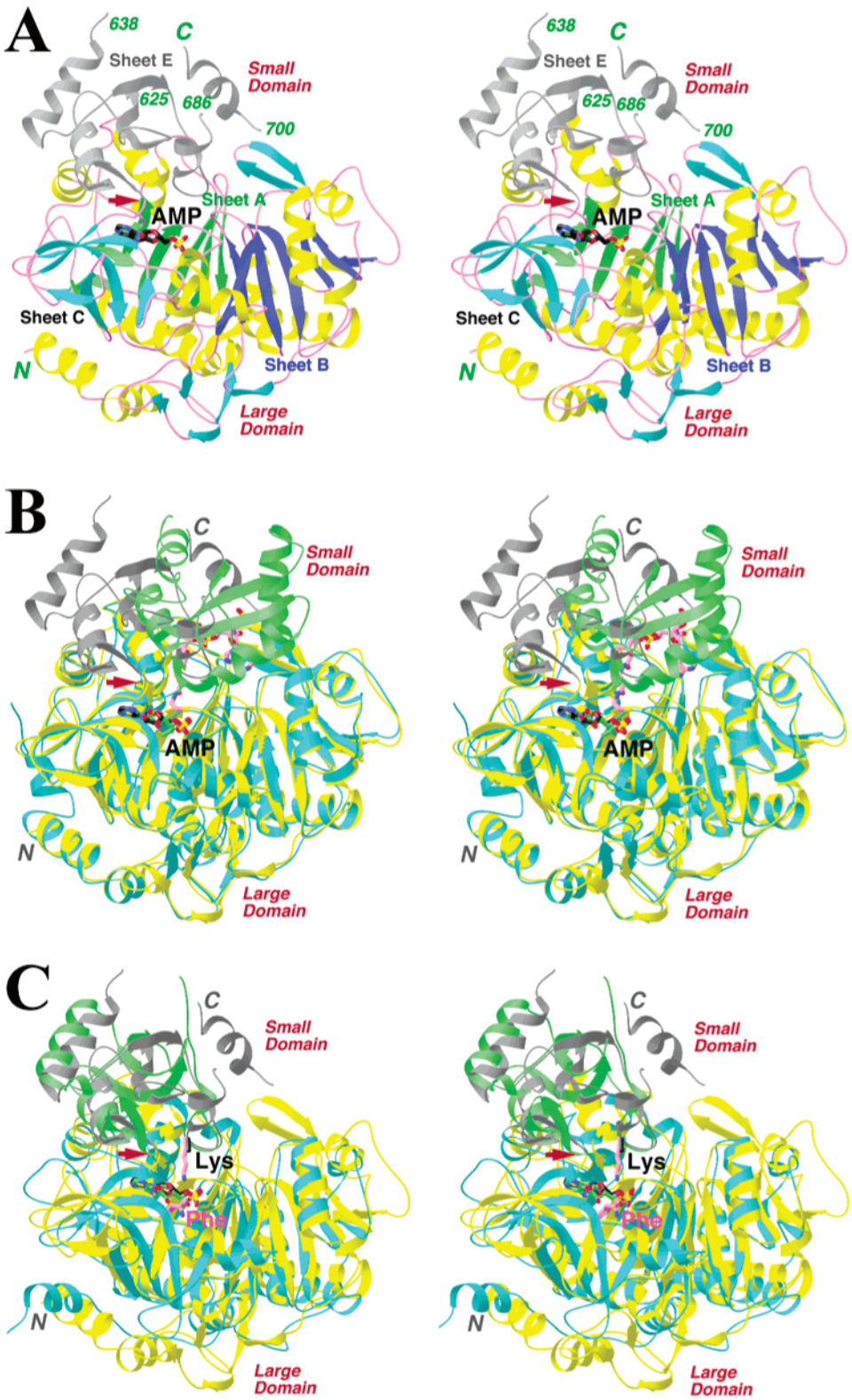

FIGURE 2: Monomer of ACS. (A) Stereodiagram showing the structure of the monomer of yeast ACS. The small domain is shown in gray. Strands in sheet A and sheet B are shown in blue and green, respectively. AMP is shown as a stick model, with black for carbon atoms. The red arrow denotes the position of the hinge residue for the movement of the small domain. (B) Stereodiagram showing the overlay of the structures of yeast ACS (yellow and gray for the large and small domains, respectively) and bacterial ACS (cyan and green, respectively) (*8*). (C) Stereodiagram showing the overlay of the structures of yeast ACS and the adenylation domain of gramicidin synthetase 1 (*6*), color-coded like panel B. The phenylalanine substrate of the latter is shown in magenta and labeled, and its active site Lys residue is also shown (magenta). The Lys675 residue (modeled as Ala) of yeast ACS is shown in black and labeled Lys. This figure was produced with Ribbons (*15*).

The hinge for the conformational change in the small domain is residue Asp576 in yeast ACS. This residue is equivalent to Asp517 in bacterial ACS, which has been identified as the hinge on the basis of the structure of that enzyme (*8*). The main chain ψ torsion angle of this residue differs by ~155° between the structures of the yeast and

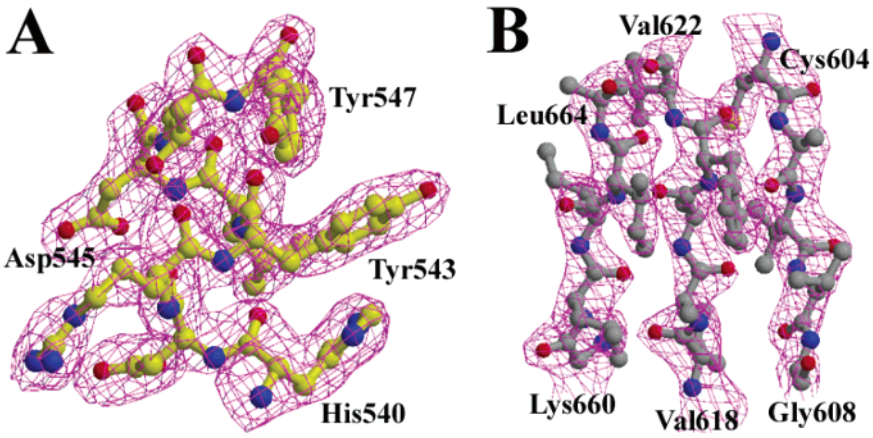

FIGURE 3: Electron density map for selected residues. (A) Final $2F_o - F_c$ electron density map at 2.3 Å resolution for residues 540−547 in the large domain. The contour level is 1σ. (B) Electron density for residues in the β-sheet of the small domain (residues 604−608, 618−622, and 660−664). This figure was produced with Molscript and Raster3D (*17*, *18*).

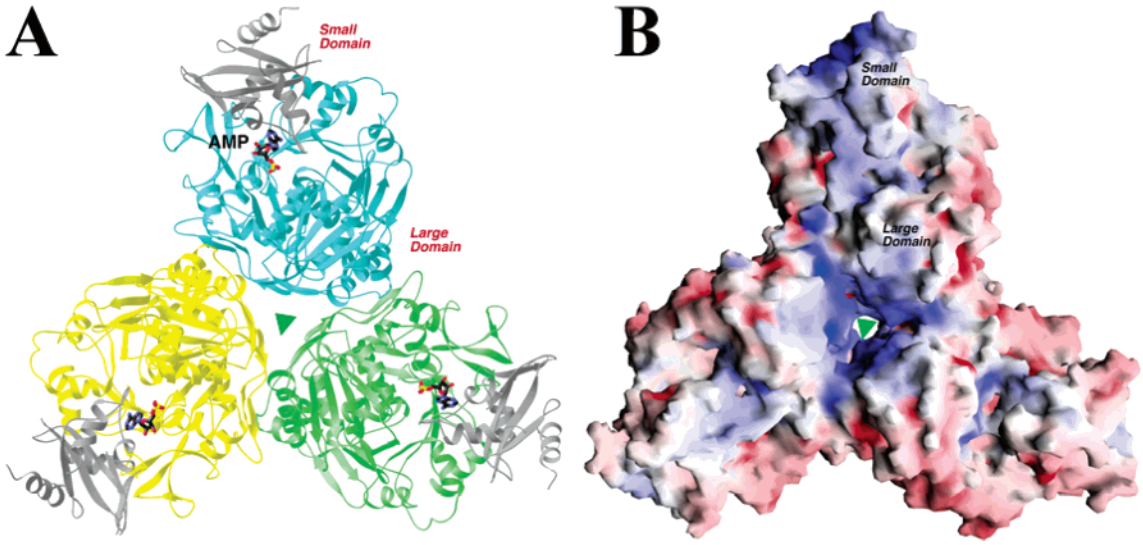

FIGURE 4: Trimer of yeast ACS. (A) The structure of the trimer of yeast ACS. The large domains are shown in yellow, cyan, and green, respectively. The small domains are shown in gray. (B) Molecular surface of the trimer of yeast ACS, viewed from the opposite direction of panel A and colored on the basis of electrostatic potential. Panel A was produced with Ribbons (*15*) and panel B with GRASP (*16*).

bacterial ACS enzymes. This leads to an abrupt change in the direction of the polypeptide change in this region of the structure (see Figure 6), and consequently a change in the position of the small domain.

Yeast ACS Is a Trimer. A trimer of yeast ACS is observed in the crystal, and this is consistent with gel filtration and light scattering studies in solution (data not shown). The trimer is formed by residues from the large domains of the three monomers only, and the small domains are located at the periphery of this oligomer (Figure 4A). Approximately 1500 Å^2 of the surface area of each monomer is buried at the trimer interface (Figure 4B).

In contrast, the bacterial ACS is a monomer (*8*). Interestingly, residues in the trimer interface of yeast ACS are poorly conserved in the bacterial enzyme (Figure 1B). This is especially true for the ^{298}KKYKTY^{303} segment, which contributes ~400 Å^2 of the surface area to the trimer interface. Examination of the amino acid sequences of the other ACS enzymes shows that the residues that are important for trimer formation are unique to yeast ACS, suggesting that this mode of trimerization may occur for this enzyme only. The biological relevance of this oligomer state of the enzyme is currently not known. The active site in each monomer is far from the trimer interface (Figure 4A).

Binding Mode of AMP. We included ATP in the crystallization solution, but the crystallographic analysis based on the diffraction data clearly shows that AMP is bound in the active site of the enzyme (Figure 5A). There is no electron density for the β- and γ-phosphates of the nucleotide. This suggests that ATP has been hydrolyzed during the crystallization process, and that our recombinant yeast enzyme has catalytic activity. Kinetic studies on the purified ACS enzyme confirm that it is catalytically active (data not shown).

AMP is bound at the interface between the large and small domains of the enzyme, although most of the interactions are with residues in the large domain (Figure 5B). The adenine base is placed between residues Glu444 and Pro445 on one side and Tyr469 on the other. The N6 amino group of adenine forms a hydrogen bond with the side chain of Asp467. The hydroxyls on the ribose are recognized by the side chain carboxylate of Asp559. One of the terminal oxygen atoms of the α-phosphate is hydrogen-bonded to the main chain amide and side chain hydroxyl of Thr472.

From the small domain, residue Lys675 is located near the AMP molecule. However, there is no electron density for the side chain atoms of this residue (Figure 5A), and it

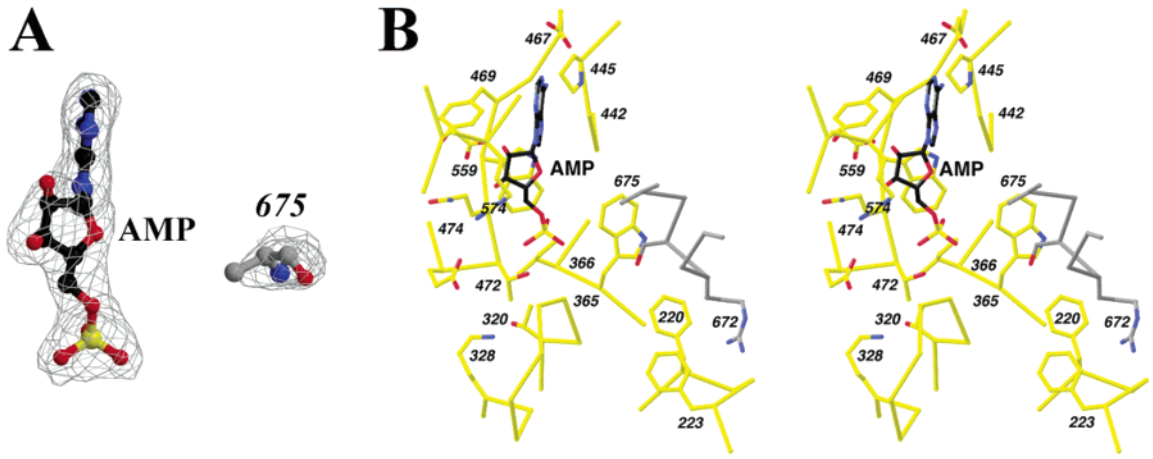

FIGURE 5: Binding mode of AMP. (A) Final $2F_o - F_c$ electron density map at 2.3 Å resolution for AMP and residue 675. The contour level is 1σ. Lys675 has no electron density for the side chain, and is modeled as Ala in the current structure. (B) Stereodiagram showing the interactions between AMP and yeast ACS. Residues in the large domain are shown in yellow for carbon atoms and those in the small domain in gray. Panel A was produced with Molscript and Raster3D (*17*, *18*) and panel B with Ribbons (*15*).

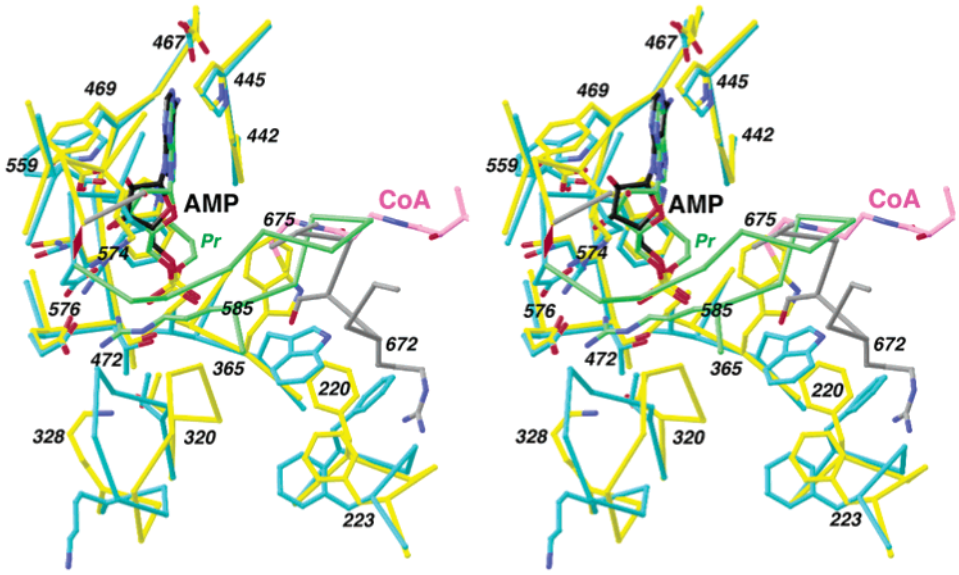

FIGURE 6: Domain reorganization and catalysis by ACS. Stereodiagram showing the active site of ACS in the binary complex with AMP (yellow and gray for the large and small domains, respectively) and in the ternary complex with propyl-AMP and CoA (cyan and green, respectively) (*8*). The CoA molecule is shown as a stick model, with magenta for carbon atoms, and propyl-AMP with green for carbon atoms. Residue numbers are for yeast ACS. This figure was produced with Ribbons (*15*).

is modeled as an Ala residue in the current atomic model. This residue is located in a highly conserved segment of ACS and other AMP-forming enzymes, and acetylation of this residue (Lys609) in the bacterial ACS inactivates the enzyme (*7*). In the structure of the adenylation domain gramicidin synthetase 1, this Lys side chain is hydrogen-bonded to the oxygen in the ribose ring, the bridging oxygen between the ribose and the α-phosphate, and the carbonyl oxygen of the substrate (*6*) (Figure 2C). This side chain is disordered in our structure probably because the substrate is not present, although the main chain of Lys675 is located at a position that is equivalent to that of the Lys residue in gramicidin synthetase 1 (Figure 2C). It is unlikely that the side chain is acetylated in our protein, as the enzyme can catalyze the hydrolysis of ATP to AMP.

Our structure is consistent with the expectation that Lys675 is a crucial residue for the first step of the reaction. Acetylation of this residue in the bacterial ACS abolishes this first step, but has little impact on the second step (*7*). In the ternary complex of bacterial ACS, this Lys residue is on the surface, away from the active site (*8*).

The binding mode of AMP in the binary complex reported here is essentially the same as that of propyl-AMP in the ternary complex of the bacterial enzyme (Figure 6) (*8*). The propyl group, a mimic for the acetyl substrate, is situated in a pocket bounded in part by Trp470. The presence of the CoA substrate in the ternary complex did not affect the binding mode of the AMP molecule (Figure 6), but it did affect the conformation of several residues in the active site (see below). The binding mode of AMP is also similar to that observed in the complex with the adenylation domain of gramicidin synthetase 1, and the phenylalanine substrate is placed in an equivalent binding pocket (*6*) (Figure 2C).

Coupling of Domain Reorganization and Catalysis. The catalysis by ACS proceeds in two steps: reaction of acetate and ATP to produce acetyl-AMP and pyrophosphate (PP_i) followed by the transfer of the acetyl group to CoA. Our binary complex with AMP may represent the form of the

enzyme that can catalyze the first step of this reaction, consistent with the presence of Lys675 in the active site in this conformation. On the other hand, the ternary complex of the bacterial ACS in complex with propyl-AMP and CoA may correspond to the enzyme conformation that can catalyze the second step (*8*). The large change in the placement of the small domain between these structures suggests that domain reorganization may be required for the catalysis by this enzyme, as has been suggested previously (*8*). It is likely that ACS can exist in both conformations (and possibly their intermediates) in solution, and efficient catalysis of the two steps of the reaction is associated with the two conformations of the enzyme observed so far.

The availability of our structure of the binary complex allows a comparison to that of the ternary complex, which illuminates the molecular mechanism for the conformational transition in this enzyme. A trigger for this domain reorganization may be the binding of the CoA substrate. The thiol group of CoA in the ternary complex sterically clashes with the side chain of Trp365 in the binary complex (Figure 6). The conformational change in this residue then induces changes for the side chains of Phe220 and Phe223, and these residues in their new positions are incompatible with the placement of residues 671−675 from the small domain (Figure 6). This is likely one of the driving forces for the repositioning of the small domain. Residue Asp576 acts as a hinge for this transition, and the residues in the small domain rotate by ∼140°. This brings residues 578−585, a β-hairpin structure that immediately follows the hinge (Figure 2A), into the active site, establishing a new ion pair between Arg585 and Glu473 (Figure 6) and moving Lys675 onto the surface of the enzyme (*8*). This domain reorganization also creates the binding site for the adenine nucleotide portion of the CoA molecule, whereas in the binary complex, the CoA binding site does not exist. The adenine base of CoA in the ternary complex sterically clashes with the side chain of Arg672 in the binary complex.

In summary, we have determined the crystal structure of yeast acetyl-coenzyme A synthetase (ACS) in a binary complex with AMP. This represents a new conformation of the enzyme, which should be able to catalyze the first step of the reaction. Lys675, from the small domain, is located in the active site in this conformation. Comparison with the structure of bacterial ACS in a ternary complex with propyl-AMP and CoA shows that the small domain undergoes a large conformational reorganization (*8*), including a rotation of ∼140°. This change leads to the formation of the CoA binding pocket, and is likely important in bringing the enzyme to a conformation that is competent for catalyzing the second step of the reaction. Yeast ACS is observed to be a stable trimer, but the bacterial ACS is monomeric. However, this trimeric oligomerization state may be unique to the yeast enzyme, as the residues in the trimer interface are poorly conserved in the other ACS enzymes.

ACKNOWLEDGMENT

We thank Benjamin Tweel for help with the enzymatic characterizations, Javed Khan, Hailong Zhang, and Xiao Tao for help with data collection at synchrotron radiation sources, and Randy Abramowitz and Xiaochun Yang for access to beamline X4A.

REFERENCES

1. Horswill, A. R., and Escalante-Semerena, J. C. (1999) The prpE gene of *Salmonella typhimurium* LT2 encodes propionyl-CoA synthetase, *Microbiology 145*, 1381−1388.
2. van den Berg, M. A., and Steensma, H. Y. (1995) ACS2, a *Saccharomyces cerevisiae* gene encoding acetyl-coenzyme A synthetase, essential for growth on glucose, *Eur. J. Biochem. 231*, 704−713.
3. Luong, A., Hannah, V. C., Brown, M. S., and Goldstein, J. L. (2000) Molecular characterization of human acetyl-CoA synthetase, an enzyme regulated by sterol regulatory element-binding proteins, *J. Biol. Chem. 275*, 26458−26466.
4. Fujino, T., Kondo, J., Ishikawa, M., Morikawa, K., and Yamamoto, T. T. (2001) Acetyl-CoA synthetase 2, a mitochondrial matrix enzyme involved in the oxidation of acetate, *J. Biol. Chem. 276*, 11420−11426.
5. Conti, E., Franks, N. P., and Brick, P. (1996) Crystal structure of firefly luciferase throws light on a superfamily of adenylate-forming enzymes, *Structure 4*, 287−298.
6. Conti, E., Stachelhaus, T., Marahiel, M. A., and Brick, P. (1997) Structural basis for the activation of phenylalanine in the non-ribosomal biosynthesis of gramicidin S, *EMBO J. 16*, 4174−4183.
7. Starai, V. J., Celic, I., Cole, R. N., Boeke, J. D., and Escalante-Semerena, J. C. (2002) Sir2-dependent activation of acetyl-CoA synthetase by deacetylation of active lysine, *Science 298*, 2390−2392.
8. Gulick, A. M., Starai, V. J., Horswill, A. R., Homick, K. M., and Escalante-Semerena, J. C. (2003) The 1.75 Å crystal structure of acetyl-CoA synthetase bound to adenosine-5′-propylphosphate and coenzyme A, *Biochemistry 42*, 2866−2873.
9. Otwinowski, Z., and Minor, W. (1997) Processing of X-ray diffraction data collected in oscillation mode, *Method Enzymol. 276*, 307−326.
10. Sali, A., and Blundell, T. L. (1993) Comparative protein modeling by satisfaction of spatial restraints, *J. Mol. Biol. 234*, 779−815.
11. Jogl, G., Tao, X., Xu, Y., and Tong, L. (2001) COMO: A program for combined molecular replacement, *Acta Crystallogr. D57*, 1127−1134.
12. Brunger, A. T., Adams, P. D., Clore, G. M., DeLano, W. L., Gros, P., Grosse-Kunstleve, R. W., Jiang, J.-S., Kuszewski, J., Nilges, M., Pannu, N. S., Read, R. J., Rice, L. M., Simonson, T., and Warren, G. L. (1998) Crystallography & NMR System: A new software suite for macromolecular structure determination, *Acta Crystallogr. D54*, 905−921.
13. Jones, T. A., Zou, J. Y., Cowan, S. W., and Kjeldgaard, M. (1991) Improved methods for building protein models in electron density maps and the location of errors in these models, *Acta Crystallogr. A47*, 110−119.
14. Tong, L. (1996) Combined molecular replacement, *Acta Crystallogr. A52*, 782−784.
15. Carson, M. (1987) Ribbon models of macromolecules, *J. Mol. Graphics 5*, 103−106.
16. Nicholls, A., Sharp, K. A., and Honig, B. (1991) Protein folding and association: insights from the interfacial and thermodynamic properties of hydrocarbons, *Proteins 11*, 281−296.
17. Kraulis, P. J. (1991) MOLSCRIPT: A program to produce both detailed and schematic plots of protein structures, *J. Appl. Crystallogr. 24*, 946−950.
18. Merritt, E. A., and Bacon, D. J. (1997) Raster3D: photorealistic molecular graphics, *Methods Enzymol. 277*, 505−524.

BI035911A